Ultrasonic/sonic drilling/coring (USDC) for planetary applications

Yoseph Bar-Cohen[a1], Stewart Sherrit[a1], Benjamin P. Dolgin[a1], Xiaqi Bao[a1], Zensheu Chang[a1], Dharmendra S. Pal[b2], Ron Krahe [b2], Jason Kroh [b2], Shu Du[b2] and Thomas Peterson[b2]

[a]Jet Propulsion Laboratory/Caltech, [b]Cybersonics, Inc.,

ABSTRACT

Future NASA exploration missions are increasingly seeking to conduct sampling, in-situ analysis and possibly return samples to Earth for further tests. Missions to Mars are the more near term projects that are seeking such capabilities. One of the major limitations of sampling on Mars and other low gravity environments is the need for high axial force when using conventional drilling. To address this limitation an ultrasonic/sonic drilling/coring (USDC) mechanism has been developed that employs an ultrasonic horn driven by a piezoelectric stack. The horn drives a free mass that resonates between the horn and drill stem. Tests have shown that the USDC addresses some of the key challenges to the NASA sampling objectives. The USDC is lightweight (450 g), requires low preload (< 5N) and can be driven at low power (5W). The device has been shown to drill rocks with various levels of hardness including granite, diorite, basalt and limestone. The hammering action involved with the coring process can produce cores of various shapes, which need not necessarily be round. Because it is driven by piezoelectric ceramics, the USDC is highly tolerant to changes in its operating environment. These actuation materials can be designed to operate at a wide range of temperatures including those expected on Mars and Venus. Although the drill is driven electrically at 20 kHz, a substantial sub-harmonic acoustic component is found that is crucial to drilling performance. An analytical model has been developed to explain this low frequency coupling in the horn, free mass, drill stem and rock.

KEYWORDS: Drilling, Coring, USDC, Planetary Sampling, Ultrasonic Drilling, In-situ Analysis

1. INTRODUCTION

Efficient drilling and coring of rock materials has a great significance to the NASA planetary program where a sample needs to be cored, in-situ analyzed, and possibly returned to Earth. Other fields can also benefit from an effective drilling, including military, medical operations, construction, geology, sport (e.g., hiking), and games. Existing drilling techniques are limited by the need for large axial forces, high power consumption, and heavy mechanisms. In addition, conventional drillers are subject to drill bit jamming, breaking, dulling and are difficult to use in non-horizontal or hard surfaces drilling. Also, the drilling process is hampered by the accumulation of drilling-debris in the drilled area. The life of coring bits is markedly reduced by the breakdown of the binder that holds the abrasive material on the bit surface. The ability of the new ultrasonic/sonic driller/corer (USDC) to operate with minimum axial load (see Figure 1) offers important enabling technology [Bar-Cohen et al., 2000]. The authors' efforts are directed towards understanding the mechanism and analytically modeling its operation thereby optimizing its performance.

FIGURE 1: A photographic view of the USDC held from its cable while coring sandstone. The minimal need for axial force is easily seen.
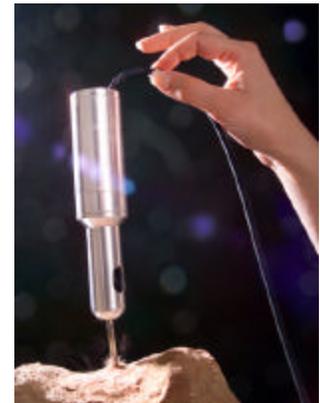
[1] JPL (MC 82-105), 4800 Oak Grove Drive, Pasadena, CA 91109-8099, Phone 818-354-2610, Fax 818-393-3254, **yosi@jpl.nasa.gov** web: **http://ndea.jpl.nasa.gov**
[2] Cybersonics, Inc., Erie, Pennsylvania, 16510-4703

To establish the required analytical model simultaneous theoretical and experimental studies have been launched and data were collected to assist in understanding the mechanism. The experimental setup consists of a USDC that is attached to a test rig as shown both schematically and photographically in Figure 2. The device consists of three main parts: ultrasonic actuator, free-mass and a drill stem. The analysis of the actuator circuit was based on the equivalent circuit of piezoelectric and acoustic elements as discussed by Mason [1948 & 1958] as was reported previously [Sherrit et al. 1999]. The horn was found to have a resonance at 21.5 kHz and the free tip velocity at resonance was determined to be linear with respect to the applied voltage and ranged from 1 to 10 m/s depending on the applied voltage and acoustic load.

FIGURE 2: Photograph and Schematic of the Ultrasonic/Sonic Driller/Corer.
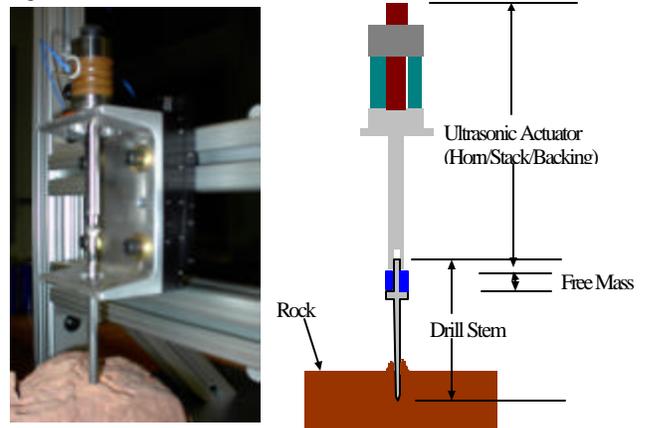
The vibrations of the horn tip excite the free-mass, which resonates between the horn tip and the top of the drill stem at frequency of the order of 1000 Hz. Acoustic energy in the free-mass resonator is transferred to the top of the drill stem and propagates to the bit/rock interface, where the rock is excited past its ultimate strain, and fractures. In order to determine the critical issues related to the control and optimization of the drill, initial modeling of the acoustic interaction at the various interfaces of the drill is presented. The three interfaces that were studied are: (1) the interaction of the horn tip with the free-mass, (2) the interaction of the free-mass with the drill stem, and (3) the interaction of the base of the drill stem (bit) with the rock.

Generally, the USDC is highly tolerant of changes in its operating environment. Because is it driven by piezoelectric ceramics the USDC can be designed to operate at a wide range of temperatures including those expected on Mars (-60 °C) and Venus (+450 °C). The operation in low temperatures was successfully demonstrated while the high temperature potential is currently being investigated. The coring bit creates a hole that is slightly larger than the drill bit diameter reducing the chances of bit jamming if the integrity of the hole is maintained, thus avoiding another problem associated with conventional drilling. The ultrasonic bit needs not be sharp and therefore it does not have problems with bit dulling and wear. Although the drill is driven electrically at 20 kHz a substantial sub-harmonic acoustic component is found that is crucial to drilling performance. An analytical model has been developed to explain this low frequency coupling interaction in the horn, free-mass behavior, drill stem, and rock.

2. MODELING

In order to proceed with the modeling, the velocity/displacement of the horn tip during operation is required. Since the velocity/displacement depends on the acoustic load, a reasonable estimate of the velocity range can determined by calculating the horn tip velocity for the case where it is free and when the acoustic impedance is perfectly matched to produce maximum power in the acoustic load. The velocity of the tip as a function of the applied peak AC voltage is shown in Figure 3 for the two cases. The reasons for using the case where the acoustic load is ideal rather than clamped are twofold. Firstly, the acoustic power transferred to the rock is substantial, which means that the horn is well matched to the rest of the acoustic elements, and secondly, in order for the device to operate efficiently a gap must be present, which means that for a substantial portion of the time the tip is not in contact with the free-mass. For a peak AC voltage of 200 Volts on the drill the velocity is found to range between 1.25 m/s for the ideal load and 13.6 m/s for the free tip. The modeling of the interaction of the free-mass can now be determined since the range of speeds of the horn tip has been set.

2.1 Horn Tip—Free-mass Interaction
The free-mass is driven by the horn tip, which vibrates at resonance frequency. A schematic of the model is shown in Figure 4. The tip displacement is harmonic and is describe by

$$u = u_0\cos(\omega t + \theta). \tag{1}$$

The velocity of the horn tip is found by taking the time derivative of the displacement and is

$$v = - \omega u_0 \sin(\omega t + \theta). \tag{2}$$

Assuming the energy loss and time duration of the impact is negligible and the mass of the horn is much larger than the free-mass, we find, using conservation of momentum and energy, that

$$v_{mf} = v_{mi} + 2v \tag{3}$$

where v_{mi} is the free-mass velocity prior to interaction with the horn and v_{mf} is the free-mass velocity after interaction with the horn. A computer simulation model, which traces the positions of the free-mass until it leaves the tip vibration range $(2u_0)$, was written. The routine calculates the free-mass speed after interaction with the horn. By keeping track of the free-mass velocity, the routine allowed us to explore this driving mechanism as a function of the horn position as the free-mass crosses the plane of full extension (phase).
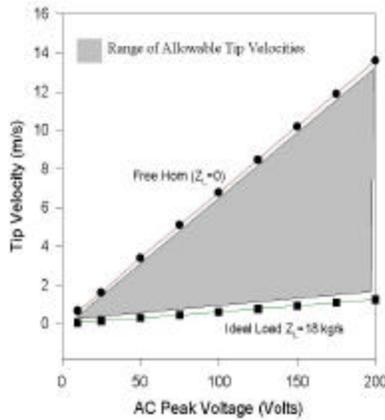

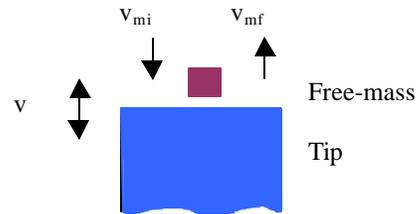**FIGURE 3:** The range of speed for the horn tip for an ideal load and for the unloaded horn.

FIGURE 4: A schematic of the free-mass horn tip interaction model.

For all cases there is a net increase in the free-mass velocity after interaction with the horn when averaged over phase. The computer model traces the movements of the free-mass and the horn. The movement of the horn is due to the reaction force on the horn tip and the force of gravity. In the calculation the mass of the free-mass is set to 1 gram, the tip velocity amplitude is set to 1.26 m/s corresponding to displacement amplitude of 10 μm. The horn mass was 800 g. The energy loss of the free-mass in each round trip is set as 75%. The simulation results shown in Figure 5 represent the ratio of the free-mass velocity to the maximum horn tip velocity as a function of time. In addition, the data was used to calculate the motion of the horn. The results show the random characteristics of the movement of the body of the horn. Figure 6 shows the horn tip position as a function of time. The motion is due to the impact interaction with the free-mass. The size, frequency and randomness of the jumps are confirmed by experimental observations of the horn tip by a high-speed camera (Figure 7).
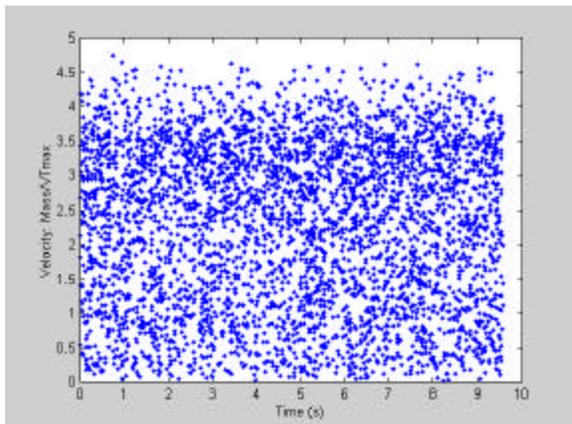

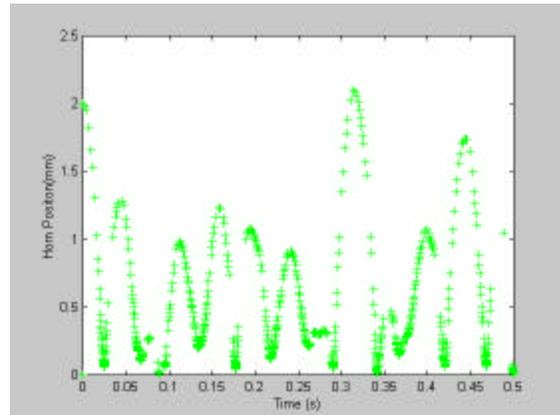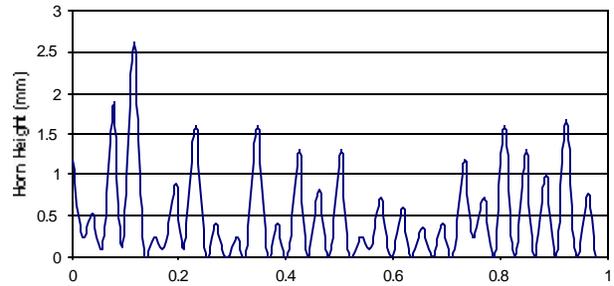**FIGURE 5:** The free-mass velocity/maximum tip velocity as

FIGURE 6: The horn position as a function of time determined

a function of time.   from model.

FIGURE 7: The horn position as a function of time
determined from high-speed camera.

2.2 Free-mass—Drill Stem Interaction

The free-mass impacts the top of the drill stem and creates a stress wave that propagates to the bit end. A finite element model was utilized to investigate the impact and resultant stress wave. Figure 8 shows results for the case where a cylindrical steel stem/bit of diameter 3.0 mm and length 100 mm with a concentric top cap of diameter 12 mm and length 6 mm. The impact used in the model is that of a free-mass of 2 g with speed 1 m/s. The free-mass has a curved surface at the contact area with a curvature of 10 mm. The free-mass is assumed to be rigid and the bit end of the drill stem is clamped. Figure 8 shows the displacement of the surface of the free-mass and the top surface of the drill stem during impact as a function of time. Figure 9 shows the resultant stress wave as a function of time at the bit end of the drill stem.

FIGURE 8: The displacement as a function of time of the free-mass and the top surface of the drill stem after impact.
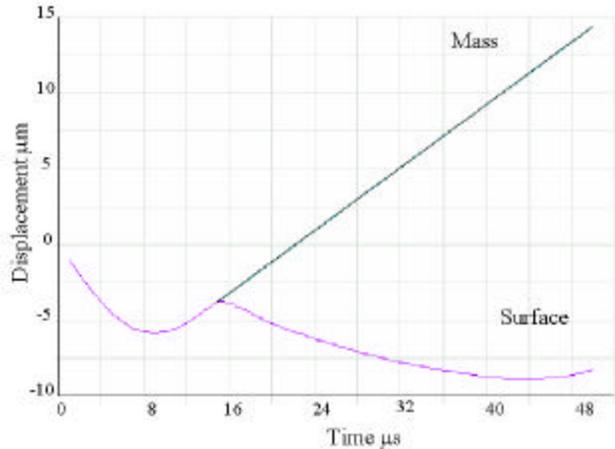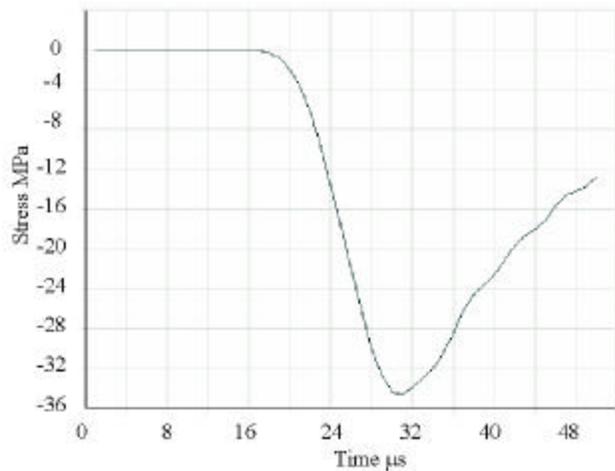

FIGURE 9: The stress as a function of time of the free-mass at the top of the drill stem after impact.

2.3   Bit-Rock Interaction

To better understand the fracture of rocks under impact loading from a drill or a corer, a finite element model was developed using ANSYS. For the purpose of simplifying the problem, the rock is modeled as a circular cylinder with bottom surface fixed and the drill/corer impacts at the center of the top surface. This simplification makes the problem axi-symmetric. By using the axi-symmetric elements available in ANSYS, the original three-dimensional problem is now reduced to two-dimensions. The

element size is made very fine near the drill/corer bit, and becomes coarser and coarser as it goes further away from the bit. Figure 10 shows a typical mesh for the problem outlined above. Preliminary results were derived by assuming that the circular cylinder is made of isotropic material with a Young's modulus of 10 GPa and Poisson's ratio of 0.3. In the case of a 3 m/s horn tip velocity the impact loading from the drill has a peak value of 0.1 GPa and duration of 25 -50 μsec, and a similar stress/time curve as shown in Figure 9.
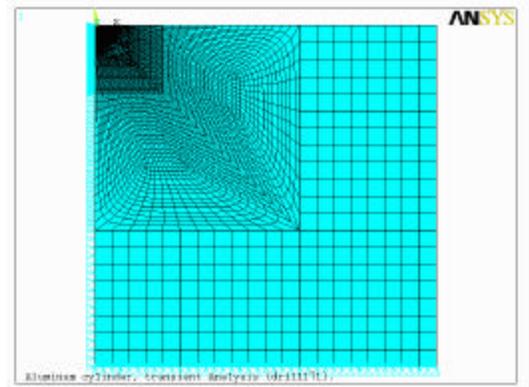

FIGURE 10: The mesh used to solve the bit rock interaction.

Contour maps of the maximum principal strain were plotted and used as indication of fracture of rocks. It also shows how the elastic waves propagate in the rock. Figures 11 show the contour maps for the cylinder for drilling and coring, respectively. The drill bit is 3 mm in diameter. The corer has an inner diameter of 2 mm and an outer diameter of 3 mm. The results shown in this Figure qualitatively illustrate the rock fracture characteristics that are induced by the ultrasonic drilling or coring. From Figure 11 we find that the highest principal strain occurs at the edge of the drill bit. Also, the highest principal strain appears at both the outer and inner edge of the corer. It implies that the fracture is likely going to happen at the edge, which is confirmed by viewing the high speed filming during drilling. By comparing the various strain profiles in Figure 11, we find that the maximum principal strain under coring is higher than that under drilling, and the area of high principal strain under coring is also larger than that under drilling. It implies that with the same outer diameter and under the same loading, a corer will drill faster than a solid drill of the same diameter. This is confirmed by experiments and the results have shown how drilling and coring can be achieved with little or no pre-load. The next challenge is to integrate each of the models to determine the limits and optimization of the USDC. Recently, the authors started seeking simplification of the models to require lower computational power than is needed for finite element models. Preliminary success was obtained when using spring-mass-damper approach offering quick solutions for the response of the free-mass and the bit interaction with the rocks. This approach was found to provide simple and fast processing time at a relatively good agreement with the FEM results. Efficient modeling will make it easier to integrate our models that simulate the motion of the free-mass, horn and drill bit. Comparison of the data for Mass-spring model and FEM for free-mass relative speed of bounce-back from the horn is shown in Figure 12.
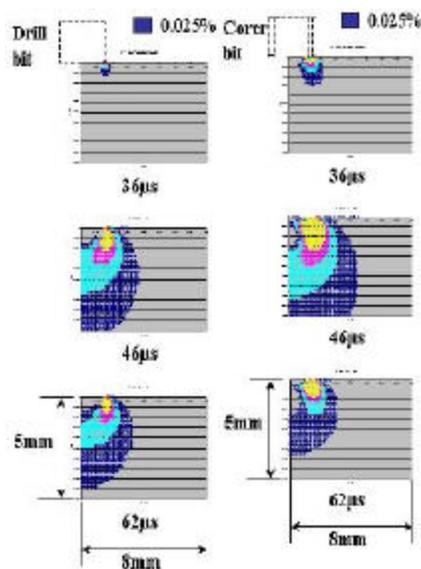

FIGURE 11: The principle strain profile at various times after impact of the free-mass on the
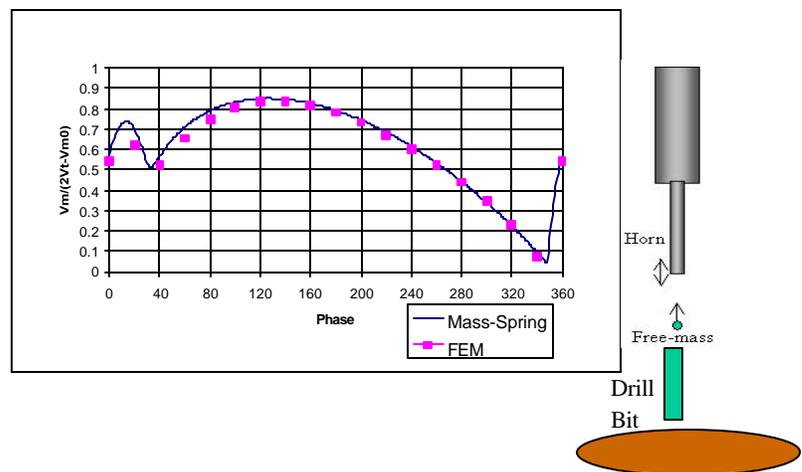
FIGURE 12: Comparison of the data for Mass-spring model and FEM for free-mass relative speed of bounce-back from the horn. The assume

drill stem for a drilling bit and a coring bit.   model of the system components is show on the right

3. Rock Sampling and Evaluation

To assure the effective applicability of the USDC to Mars exploration, it is necessary to determine its ability to sample rocks and that the produced tailing will have minimum destruction of its original features. Jointly with JPL geologists, rocks with mechanical properties as expected on Mars were selected. Using the test fixture that was shown in Figure 2, the selected rocks were sampled and the rock tailing was collected for analysis. In parallel drilling performance data was acquired to allow determining the efficiency of the USDC. This test was conducted using 12-Watts average power (24 Watts peak power- 50% duty cycle). The power was measured at the input of the electronics and includes the circuitry loss of the driving electronics. For these data the drilling depth as a function of time can be describe by the functional relationship

$$D(t) = D_0 t^n \tag{4}$$

where D_0 and n are constants that depend on the drill bit geometry and the rock type for a given power level. The value of the constant n is between 0 and 1. The drill rate can be determined by taking the time derivative and it is

$$R(t) = nD_0 t^{n-1} \tag{5}$$

The rate is seen to decrease as a function of the time (depth). This saturation is likely due to a combination of causes including the collection of tailings at the face of the bit damping the impact on the rock, viscous drag of the tailings on the drill stem, and non-linear elastic properties of the rock .

In order to determine if the drilling action alters the rock mineralogy four samples of drill tailings from each type were collected from the USDC after they were transported from the hole by the ultrasonic mechanism and compared with the powder produced by conventional lab grounding for the same materials. Five different rock samples were chosen for this study including Iron Oxide, 2 Iron Oxyhydroxides samples, Pyroxene and a Carbonate sample. An example of the rock abrasion tools is shown in Figure 13. The letters JPL were carved into the basalt using the tungsten carbide coated sphere in approximately 40 minutes using 12 watts power (29 kJ) which is a factor of 2 to 3 less energy than conventional abrassion tools. The circular area below and to the right was carved using the 2D array of pyramidal bits. Further, it was shown that X-ray diffraction analysis reveals similar results with a difference that is attributed to the particle size difference between the samples that are produced by USDC and conventional lab grinding.

FIGURE 13. Basalt rock sample tested using the abrasion tools.

4. Operation from Various Platforms

Given the low axial force that is needed to drill with the USDC, a series of demonstrations were made to show the feasibility of this technology to supporting exploration missions. To examine its performance from the Sojourner Rover (see Figure 14) a tube used as a guide through which the USDC was inserted and allowed to operate using its own mass as the load. The tube internal diameter was about 3 mm larger than the external diameter of USDC and the USDC was easily shown to make holes and cores in various rocks (basalt, sandstone, etc.). Also, the device was mounted onto the robotic arm of the FIDO rover (see Figure 15) and drilled with minimal mechanical vibration of the arm and was easily used to reinsert the drill bit into holes that were drilled earlier. The ability of the USDC to drill under low axial load has also made it possible to consider operating from an aerobot or inflatable systems using minimal anchoring.

5. Conclusions

A new drilling and coring method was reported allowing operating with low power and needing low axial force. The drill was activated from such platforms as the Sojourner Rover and the robotic arm of the FIDO Rover. By combining resonant elastic

vibrations at 20 KHz and inducing a substantial sub-harmonic acoustic component, significant impact force and displacement are generated. The phenomenon is induced by a stack of piezoelectric wafers using an ultrasonic horn and a free-mass that is interfaced with the drill bit. Analytical models were developed to explain the low frequency coupling between the horn, free-mass, drill stem and rock. Current efforts are underway to integrate the various models to allow for the determination of system model with predictive and control abilities. The results suggest a variety of avenues for optimization of the device.

This new drilling and coring device was demonstrated to require a relatively low preload ($< 5N$) and can be driven at low power (5W). It was used to drill rocks as hard rocks as granite, diorite, basalt and as soft as limestone and sandstone. This USDC has enabled new possibilities in support of future NASA missions including sampling, as well as in-situ probing and analysis. Given the wide range of performance of piezoelectric materials it is suggested that a drill can be developed for operation at both high and low temperatures allowing sampling in harsh enviroments such as the planet Venus.

FIGURE 14: The USDC mounted on the Sojourner Rover platform is shown to drill sandstone.

FIGURE 15: The USDC is shown drilling while mounted on the robotic arm of the FIDO Rover

Acknowledgment

References

Bar-Cohen Y., S. Sherrit, B. Dolgin, T. Peterson, D. Pal, J. Kroh, and Ron Krahe, "Smart Ultrasonic/Sonic Driller/Corer (SUSDC)," Provisional Patent, filed on May 3, 2000, Application No. 60/201,650 (2000).

Mason W. P*., Electromechanical Transducers and Wave Filters*, Princeton, NJ, Van Nostrand, 1948.

Mason W. P., *Physical Acoustics and the Properties of Solids*, D. Van Nostrand Co., Princeton, NJ, 1958.

Sherrit S., B. P. Dolgin, Y. Bar-Cohen, D. Pal, J. Kroh, T. Peterson "Modeling of Horns for Sonic/Ultrasonic Applications," Proceedings of the IEEE International Ultrasonics Symposium, Lake Tahoe, CA, October 1999, pp. 647–651.